Dissociative Photodetachment Dynamics of $S_2O_2^-$

Todd G. Clements, Hans-Jürgen Deyerl,[†] and Robert E. Continetti*

Department of Chemistry and Biochemistry, University of California, San Diego, 9500 Gilman Drive, La Jolla, California 92093-0340

Photoelectron-photofragment coincidence spectroscopy is employed to study the dissociative photodetachment (DPD) dynamics of $S_2O_2^-$ at 258 nm. Experimental data and theoretical calculations show evidence for photodetachment from a trigonal form of $S_2O_2^-$. The vertical detachment energy of this isomer was determined to be 3.73 ± 0.02 eV. An upper bound of 2.41 ± 0.14 eV is determined for the enthalpy of the reaction $S_2O_2^- \rightarrow S + SO_2 + e^-$ at 0 K. The observed dynamics are interpreted in terms of dissociative photodetachment of $S_2O_2^-$ to $S(^3P) + SO_2(^1A_1) + e^-$, $S(^1D) + SO_2(^1A_1) + e^-$, and $S_2(^3\Sigma_g^-) + O_2(^3\Sigma_g^-) + e^-$ product channels. The S-atom channels are characterized by a large photofragment kinetic energy release and an anisotropic photofragment angular distribution peaked along the electric vector of the laser. The S_2 channel has a low kinetic energy release consistent with elimination of highly vibrationally excited O_2 from a strained form of the trigonal isomer.

1. Introduction

Sulfur monoxide (SO) acts as an intermediate in the oxidation of sulfur compounds in combustion[1] as well as the atmosphere.[2] It may also be an important participant in the atmospheric chemistries of Venus[3] and Io.[4] As a result, the energetics and reaction dynamics of this molecule are of considerable interest. Herron and Huie studied the kinetics of formation of the transient SO dimer (S_2O_2), created by the reaction SO + SO + M → $(SO)_2$ + M and concluded that the $(SO)_2$ cluster is relatively long-lived.[5] Harcourt proposed that a triplet S_2O_2 intermediate plays a role in the formation of SO_2 and S_2O from SO.[6] The stability and dissociation dynamics of these intermediates can have a significant effect on interpretations of the chemical kinetics of SO,[5] but experimental information on these clusters is scarce. Photoelectron photofragment coincidence (PPC) spectroscopy has been shown to be a valuable method for studying the energetics and dissociation dynamics of transient neutral molecules after photodetachment from the anion.[7,8] In this paper, PPC spectroscopy is applied to $S_2O_2^-$, and represents the first investigation involving the anionic form of this molecule.

There have been a number of previous spectroscopic studies of neutral S_2O_2. Lovas et al. observed S_2O_2 in a microwave discharge of SO_2.[9] In those experiments, S_2O_2 was found to have a cis-planar OSSO structure similar to that in Figure 1a. A number of theoretical studies have been performed on S_2O_2[10−13] and although only the cis-planar structure has been observed experimentally, Marsden and Smith calculated thirteen singlet and six triplet isomers of S_2O_2.[10] They concluded that a trigonal planar form of S_2O_2 (Figure 1b), similar in structure to SO_3 is more stable than the cis-planar isomer, but was not observed in the microwave discharge spectra due to the relatively high energies of molecular products from that method. The photoionization efficiency spectrum of S_2O_2 has also been measured in the range 650−1250 nm[14] and 105−130 nm,[15] with

† Current address. Research Center COM, DTU, DK-2800 Kgs. Lyngby, Denmark.
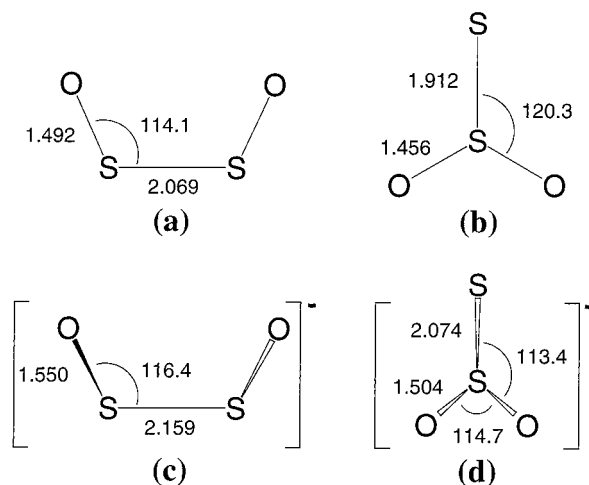* Corresponding author. E-mail: rcontinetti@ucsd.edu.

Figure 1. Calculated geometries of S_2O_2 at the B3LYP/6-311+G(d) level. (a) cis-planar S_2O_2, (b) trigonal planar S_2O_2, (c) cis-OSSO⁻ (the SO bond is rotated by 40.3° out of plane), and (d) trigonal $S_2O_2^-$. Distances are given in Å, and bond angles in degrees.

the latter study yielding an adiabatic ionization energy of 9.93 ± 0.02 eV.

We present the photoelectron spectrum, the energy-dependent photofragment angular distribution, and the photoelectron photofragment correlation spectrum of the anion $S_2O_2^-$. From these data we show evidence for the trigonal isomer of $S_2O_2^-$ (Figure 1d) and determine the energetics and dynamics of the dissociation of the corresponding neutral (Figure 1b).

2. Experimental Section

The photoelectron photofragment coincidence spectrometer has been described before in detail[16] and will be reviewed only briefly here. The source gas configuration differs from previous descriptions of this technique. Here, $S_2O_2^-$ is produced by electron impact on two crossed continuous gas expansions, similar to (although simpler than) entrainment methods used by Johnson and co-workers[17] and discussed in early supersonic-

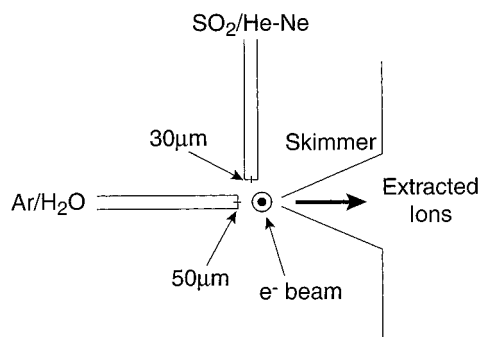**280** *J. Phys. Chem. A, Vol. 106, No. 2, 2002*

Clements et al.

Figure 2. Schematic of the dual beam continuous gas source. The bulk of the gas jet is argon from the 50 μm nozzle which lies along the ion beam axis of the machine.

TABLE 1: Bond Lengths (Å) and Angles (degrees) for Trigonal and cis-OSSO S_2O_2 at the B3LYP/6-311+G(d)[a] and SCF/DZ(P)[b] Levels

	r(SO)	r(SS)	$\angle$OSS
trigonal			
B3LYP	1.492	2.069	114.1
SCF	1.471	1.931	114.3
cis-OSSO			
B3LYP	1.456	1.912	120.3
SCF	1.426	1.866	120.5

[a] Present work. [b] Ref 10.

beam literature.[18] Along the ion-beam axis of the machine, pure argon at 25 psi backing pressure is passed over room-temperature water and expands through a 50 μm nozzle. Perpendicular to this beam, a mixture of 6% SO_2 seeded in 28% Ne and 66% He at 50 psi backing pressure is expanded through a 30 μm nozzle. A schematic of this setup is shown in Figure 2. Although a continuous expansion may be expected to produce anions at a higher temperature than a pulsed expansion, a previous study of $O^-(H_2O)_2$ showed no change in the experimental results, such as the width of features in the photoelectron spectra, between the two sources.[19] However, $O^-(H_2O)_2$ can be cooled via solvent evaporation, which may not be the case for $S_2O_2^-$. The effects of photodetachment from vibrationally excited anions on the experimentally determined energetics will be discussed. The anions are collisionally cooled in the jet and pass through a skimmer where they are accelerated to 4−6 keV and chopped into packets at a repetition rate of 1 kHz by a pulsed high voltage switch. The ions are mass selected by time-of-flight and guided into the interaction region where particles with $m/e = 96$ are intersected by the third harmonic (258 nm, 4.80 eV, 1.2 ps fwhm) of a regeneratively amplified Ti:sapphire laser (Clark, MXR CPA-2000) which provides a fluence of 4−8 mJ/cm^2 per pulse.

Photodetached electrons are detected by one of two large-solid-angle time- and position-sensitive electron detectors. The time and position information is used to transform the laboratory kinetic energy into a center-of-mass (CM) electron kinetic energy (eKE) to remove the Doppler shift arising from the high speed of the incident anion beam. The electron detectors have been shown to have an eKE resolution of $\Delta E/E \approx 5\%$ at 1.3 eV[20] and are calibrated using the photodetachment of I$^-$. Assuming a cold anion beam, determination of the eKE for each event fixes the energy in the photodetached neutral complex.

The dissociating neutral fragments recoil out of the fast beam and travel along a 104 cm flight path until they impinge on a microchannel-plate-based time- and position-sensitive neutral particle detector. The anode is composed of four independent crossed delay lines each capable of measuring two particles per event. The number of particles analyzed for each event is determined by gating on the total charge from the microchannel plates of the neutral particle detector, easily resolving detection of one, two, or three neutral fragments. Conservation of linear momentum in the CM frame is used to determine the mass ratio of the products in a two-body dissociation. Once the mass ratio has been calculated, the CM translational energy of the neutral particles (E_T) can be calculated from the time- and position-of-arrival of the two particles, the incident beam energy, and the flight path from the interaction region. The recoil angle and energy of the photoproducts relative to the photodetachment

laser is recorded on an event-by-event basis which allows direct determination of the energy-dependent anisotropy of the dissociation as discussed below. This detector has effectively no dead area within the active region and has a resolution of ∼11% $\Delta E/E$ at 0.7 eV measured using the photodissociation of O_2^-.
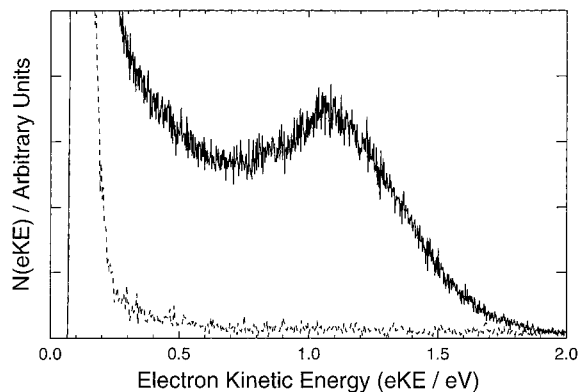
3. Calculations

To aid in the interpretation of these results, electronic structure calculations were performed using the Gaussian 98[21] suite of programs. Geometries of the anion and neutral were optimized using density functional theory (DFT) employing the correlation functional of Lee, Yang, and Parr[22] with the exchange functional of Becke[23] (B3LYP) and the Pople valence triple-ζ basis set including polarization and diffuse functions (6-311+G(d)).[24] The diffuse functions are required for accurate calculations on the anion geometry. Frequency calculations were performed at the same level and single-point energy calculations were performed using the same basis set with the quadratic configuration interaction, QCISD(T),[25] and coupled cluster, CCSD(T),[26] methods, both employing single, double, and triple substitutions. To determine the vertical detachment energy (VDE), the energy of the neutral was also calculated at the anionic geometry. The zero-point energies calculated at the B3LYP/6-311+G(d) level were appropriately scaled[27] and used to correct the absolute energies of all methods used in this study.

Figure 1 shows calculated geometries for the S_2O_2 neutral and anion in both the cis-OSSO and trigonal geometries. In both cases, the ground-state neutrals are in singlet electronic configurations and the anions are doublets. DFT B3LYP/6-311+G-(d) calculations showed that the anion quartet states were much higher in energy: 2.7 and 1.8 eV for the cis-OSSO and trigonal geometries, respectively. There is a large geometry change between the ground-state anion and neutral in both isomers. In the case of the cis-OSSO anion geometry, addition of the electron causes an out-of-plane rotation of 40.3° around the S−S bond and lengthening of the S−S and S−O bonds. In the trigonal geometry, the anion takes a pyramidal shape, as seen in both SO_3^-[28] and CF_3^-.[29] However, unlike SO_3^- and CF_3^-, $S_2O_2^-$ undergoes dissociative photodetachment at 258 nm. The DFT geometries for the neutral molecules differ from those calculated by Marsden and Smith optimized at the SCF level and employing a double-ζ basis set with polarization functions only on the S atoms.[10] The geometries determined from both calculations are summarized in Table 1. The largest difference between the two calculations is the S−S bond length which increased from 1.931 to 2.069 Å for the trigonal isomer, and from 1.866 to 1.912 Å for the cis-OSSO isomer. For this bond in the cis-OSSO isomer, the DFT value more closely matches the experimental value of 2.025 Å.[9] Given the larger basis set employed in the present calculation, which included both polarization and diffuse functions on both O and S, the closer agreement with experiment is expected. Vibrational frequencies

TABLE 2: Theoretical Vibrational Frequencies (cm^{-1}) for Neutral and Anionic cis-OSSO and Trigonal-S_2O_2 at the B3LYP/6-311+G(d) Level

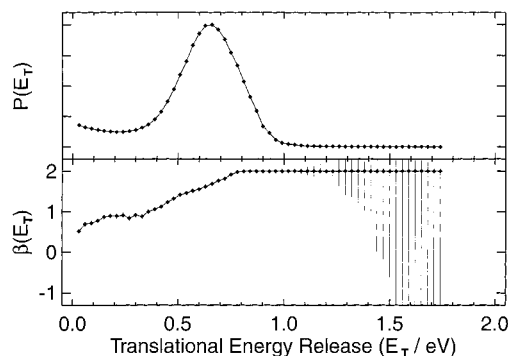|	cis-OSSO$^-$	cis-OSSO		trigonal $S_2O_2^-$	trigonal S_2O_2
OSSO sym wag	133	140	SO_2 wag	280	356
OSSO torsion	185	255	SS str	331	625
OSSO asym wag	367	451	umbrella	434	367
SS str	376	447	SO_2 bend	490	445
SO asym str	916	1087	SO sym str	972	1114
SO sym str	968	1138	SO asym str	1096	1301

Figure 3. Photoelectron spectrum, $N(eKE)$, of $S_2O_2^-$. Below 0.3 eV, laser background contributes significantly to the spectrum and is removed. The laser polarization is parallel to the electron detector face.

for both the neutral and anionic forms of each isomer are presented in Table 2.

4. Results

Figure 3 shows the photoelectron spectrum of $S_2O_2^-$. The cutoff at low energies is a result of electron background from the laser striking surfaces inside the machine. This background is plotted as the dotted line and is estimated by recording and analyzing electron events which occur when the anion beam is not present. The spectrum is characterized by one broad feature centered at 1.07 ± 0.02 eV, and the appearance of another broad feature which extends into the laser background. With the current experimental setup, it is not possible to distinguish between the possible candidates for $m/e = 96$ in the incident anion beam: S_3^-, $S_2O_2^-$, SO_4^-, and O_6^-. However, published photoelectron spectra exist for each of these compounds other than $S_2O_2^-$. For S_3^- Nimlos and Ellison observed features at a minimum binding energy of 2.106 ± 0.014 eV, with more intense features appearing at 2.297 ± 0.005 eV.[30] These binding energies would correlate to features at 2.7 and 2.51 eV, respectively, in the PES spectrum in Figure 3. These peaks are not observed and the onset of the presented spectrum is approximately 2.0 eV, well below that of S_3^-. SO_4^- has a vertical detachment energy (VDE) of 5.4 ± 0.1 eV[31] and would thus not be subject to photodetachment at the current photon energy of 4.80 eV. A 266 nm (4.66 eV) photoelectron spectrum of O_6^- shows features as high as 3.4 eV and also shows three body DPD, unlike the current system.[20,32] There is no evidence in the photoelectron spectrum for ionic photodissociation yielding S^-, S_2^-, SO_2^-, S_2O^-, or O^- products which may undergo photodetachment by a second photon during the 1.2 ps laser pulse.

Figure 4 shows the photofragment translational energy release, $P(E_T)$, and the energy-dependent anisotropy parameter, $\beta(E_T)$, for the DPD of $S_2O_2^-$. Owing to the effectively zero dead space design of the detector as well as the dynamics of $S_2O_2^-$ DPD,

Figure 4. Product translational energy distribution, $P(E_T)$, and the energy-dependent anisotropy parameter, $\beta(E_T)$, of the dissociative photodetachment of $S_2O_2^-$. The x-axis is the photofragment translational energy (E_T) and the y-axis is the value of the anisotropy parameter, β, for a given E_T. Uncertainties in the $\beta(E_T)$ fit are shown as vertical lines for each point.

the experimentally measured photofragment translational energy release distribution, $N(E_T)$, very closely matches the actual $P(E_T)$ distribution. As a result, detector acceptance function (DAF) correction methods which have been employed previously to transform $N(E_T)$ into $P(E_T)$ are not necessary for the current study and $P(E_T)$ is reported directly.[33] Immediately visible in the $P(E_T)$ spectrum are low and high E_T regions; the low E_T component extends to and peaks near 0 eV, while the high E_T component peaks at 0.66 ± 0.02 eV. As discussed below, these two regions are assigned to two different dissociation channels for S_2O_2. $\beta(E_T)$ is determined by fitting to the electric dipole model:[34,35]

$$P(E_T, \theta) = P(E_T)[1 + \beta(E_T)P_2(\cos \theta)] \qquad (1)$$

where $P(E_T)$ is the photofragment translational energy release distribution and $P_2(\cos \theta)$ is the second-order Legendre polynomial in $\cos \theta$. $\beta(E_T)$ can vary from -1 to $+2$, where a value of -1 corresponds to a $\sin^2 \theta$ (perpendicular) distribution of photofragments around the polarization of the laser, and $+2$ corresponds to a $\cos^2 \theta$ (parallel) distribution. The energy-dependent anisotropy parameter, $\beta(E_T)$, shown in Figure 4 has two discernible regions. The first region is $E_T = 0.0-0.4$ eV, where there is a roughly linear increase from $\beta = 0.5-1.0$, a somewhat parallel distribution of photofragments. The slope of $\beta(E_T)$ changes around $E_T = 0.4$ eV and from 0.4 to 0.8 eV, there is again a linear increase from $\beta = 1.0-2.0$, a highly parallel transition ($\cos^2 \theta$ distribution). Above 0.8 eV translational energy, β remains at 2.0. The two regions from $E_T = 0.0-0.4$ eV and > 0.4 eV are correlated with the two regions of the kinetic energy spectrum and are likely from two different dissociation pathways available to S_2O_2. The mass spectrum for this dissociation, not presented here, shows two peaks at 32 and 64 amu. There is no evidence of dissociation into $SO + SO$ or $O + S_2O$; events with either of these mass ratios comprise less than 4% of the total events, compared to the estimated 5% false coincidence rate for these experiments.[16] Using charge gating as described in the Experimental Section, no evidence was seen for either stable S_2O_2 or dissociation into more than two particles.

Figure 5 shows the photoelectron-photofragment correlation spectrum for the DPD of $S_2O_2^-$. The y-axis represents the electron kinetic energy, the x-axis the total photofragment kinetic energy, and the contours represent the number of events, $N(E_T, eKE)$, with a given correlated electron kinetic energy and

TABLE 3: Theoretical Energies and Experimental Adiabatic Electron Affinity (AEA) and Vertical Detachment Energy (VDE) for S_2O_2. Energies in Hartrees except as Noted

	B3LYP/ 6-311+G(d)	ZPE B3LYP/ 6-311+G(d)[a]	QCISD(T)/ 6-311+G(d)	CCSD(T)/ 6-311+G(d)	exptl
trigonal (Figure 1b,d)					
anion energy	−946.9405046	0.008207	−945.5134903	−945.5110435	
neutral energy	−946.8350458	0.009541	−945.4288651	−945.4264558	
neutral at anion geometry	−946.7980913		−945.3946611	−945.3913160	
AEA (eV)	2.91		2.34	2.34	
VDE (eV)	3.91		3.27	3.29	3.73 ± 0.02
cis-OSSO (Figure 1a,c)					
anion energy	−946.9218950	0.006704	−945.4904741	−945.4873157	
neutral energy	−946.8336924	0.008014	−945.4299987	−945.4266325	
neutral at anion geometry	−946.8147325		−945.4160162	−945.4117131	
AEA (eV)	2.44		1.69	1.68	
VDE (eV)	2.95		2.09	2.06	

[a] Zero-point energy (ZPE) corrections for the QCISD(T) and CCSD(T) levels taken from the B3LYP calculations (and are scaled by 0.9806 (ref 27) for AEA and VDE calculations). The zero-point energy for the neutral was used for the neutral calculated at the anion geometry.
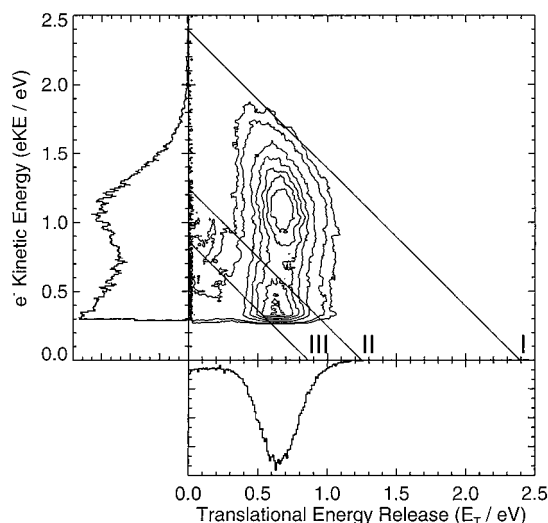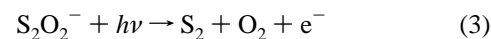

Figure 5. Photoelectron-photofragment correlation spectrum, $N(E_T,eKE)$, for $S_2O_2^-$. Each point represents the correlated photoelectron kinetic energy and photofragment translational energy release for a DPD event. Lines (I) and (II) represent the maximum energy available for the reaction $S_2O_2^- + h\nu \rightarrow S + SO_2 + e^-$ producing S(^{3}P) and S(^{1}D), respectively. Line (III) represents the maximum energy available for the reaction $S_2O_2^- + h\nu \rightarrow S_2 + O_2 + e^-$. To better visualize the small amount of lower kinetic energy data, the first two contours are drawn at 5% and 10%, increasing by 15% for each successive contour.

photofragment kinetic energy. The E_T and eKE plots are generated by integrating over the conjugate variable in the correlation spectrum. As in the photoelectron spectrum, electron energies below 0.30 eV are removed owing to strong laser background. Due to conservation of energy, a diagonal line can be drawn at KE$_{MAX}$ (I) representing the maximum translational energy release available for DPD. If it is assumed that this maximum kinetic energy corresponds to products in their ground electronic and vibrational states, any events occurring below this line are representative of product rovibrational or electronic excitation. KE$_{MAX}$ = 2.39 eV is drawn at the 5% false-coincidence contour level giving an estimated energy of 2.41 ± 0.06 eV for the DPD reaction

$$S_2O_2^- + h\nu \rightarrow S(^3P) + SO_2(^1A_1) + e^- \quad (2)$$

Two additional diagonal lines are drawn at 1.24 eV (II) and 0.86 eV (III), where (II) represents KE$_{MAX}$ for production of S(^{1}D) in reaction 2 and the difference in energy between (I) and (III) is given by the 0K heat of reaction for S(^{3}P) + SO$_2$ →

$S_2(^3\Sigma_g^-) + O_2(^3\Sigma_g^-)$ of 1.53 eV.[36] This limit corresponds to KE$_{MAX}$ for the DPD process

$$S_2O_2^- + h\nu \rightarrow S_2 + O_2 + e^- \quad (3)$$

5. Discussion

The photoelectron spectrum of $S_2O_2^-$ shows no vibrational resolution despite the fact that a stable neutral isomer is known to exist. Since no stable S_2O_2 was found and a highly anisotropic product angular distribution was observed, photodetachment must be occurring to a repulsive portion of the potential energy surface (PES) of neutral S_2O_2. Given the large geometry change between the anion and the neutral, photodetachment outside of the stable well is not unexpected. Photodetachment to a repulsive region of the PES is also consistent with the large E_T seen in Figure 4. The vertical detachment energy (VDE) is 3.73 ± 0.02 eV based on the 1.07 ± 0.02 eV peak and the 4.80 eV photon energy.

Single-point energy calculations on the anionic and neutral ground states were performed at three different levels of theory using the B3LYP/6-311+G(d) optimized geometry and compared to experimental energetics. The results of these calculations for the adiabatic electron affinity (AEA) and VDE are presented in Table 3. An experimental value for the AEA of S_2O_2 is unknown, and is difficult to estimate from the data which results from photodetachment to a repulsive electronic state. The predicted AEA and VDE of the trigonal isomer are larger than those of the cis-OSSO isomer for all three levels of theory. The difference between the AEA and the VDE for both isomers reflects the large geometry change of the isomers between the anion and neutral, and is larger in the case of the trigonal isomer which undergoes more significant rearrangement between the neutral and anionic forms. The theoretical values of the VDE can be compared to results from the present experiment. In all cases except for the B3LYP energetics for the trigonal isomer, the calculated VDE is smaller than the experimental value. At the CCSD(T) level, the calculated VDE is 0.44 eV lower than the experimental value for the trigonal isomer and 1.67 eV lower for the cis-OSSO isomer. Given the significantly better agreement between the experimental and theoretical VDE for the trigonal isomer, the calculations are consistent with photodetachment from the trigonal anion. However, calculations involving second row atoms and open shell anionic species are difficult, and can thus only be used as a guide.

Overall, the DPD of $S_2O_2^-$ at 258 nm leads to a large E_T, similar to that seen in the analogous $N_2O_2^-$ anion.[37] $P(E_T)$ peaks at 0.66 ± 0.02 eV, but also has a component at lower kinetic

energies. The large E_T component must result from photodetachment to a highly repulsive region of the neutral potential surface, a fact confirmed by the observation of a anisotropic angular distribution close to the limiting value of 2.0 at large E_T. The ΔH_f of S_2O_2 is unknown, but given that the reaction $SO + SO + M \rightarrow (SO)_2 + M$ occurs,[5] $\Delta H_f(S_2O_2)$ must be less than the heat of formation of the two SO reactants: $\Delta H_f(S_2O_2) \leq \{2 \cdot \Delta H_f(SO) = 10.06 \text{ kJ/mol}\}$.[36] Using this ΔH_f, the reaction $S_2O_2 \rightarrow S(^3P) + SO_2(^1A_1)$ is exothermic by at most 29.63 kJ/mol (0.31 eV). The photoelectron spectrum, peaking at eKE = 1.07 eV, however, shows that the nascent neutral S_2O_2 is produced ~1.3 eV above the $S(^3P) + SO_2(^1A_1)$ dissociation asymptote at the peak of the distribution, providing significant available energy for product translation.

The photoelectron-photofragment correlation spectrum shown in Figure 5 provides important insights into the product channels and dissociation dynamics. Three regions are visible in the spectrum, two centered above the high E_T peak, and one above the low E_T peak. The diagonal lines correspond to the energetic limits for creation of (I) $S(^3P) + SO_2(^1A_1)$, (II) $S(^1D) + SO_2(^1A_1)$, and (III) $S_2(^3\Sigma_g^-) + O_2(^3\Sigma_g^-)$ as discussed in the results section. Features (II) and (III) match well the two lower energy features of the correlation spectrum. This correspondence with the known energy differences between these plausible product channels provides confidence in the assignment and also implies that photodetachment is occurring from a single isomer of $S_2O_2^-$. This can be contrasted with the case of $N_2O_2^-$, where evidence for two isomeric forms of the anion was obtained from the correlation spectra for different product channels.[37] It is proposed that the reactions are occurring from a trigonal anionic geometry as seen in Figure 1d. There is no easily accessible pathway from cis-OSSO⁻ (Figure 1c) to form $S + SO_2$, which is the lowest energy dissociation pathway. It is conceivable that a cyclic structure could allow for creation of S + OOS products, but formation of OOS, calculated to lie more than 4 eV higher than OSO,[38] is not energetically accessible at this wavelength. On the other hand, for the trigonal structure, formation of mass 32 and mass 64 products can proceed by fission of a single S−S bond. The highly parallel photofragment angular distribution also implies a simple bond fission with the transition moment in the direction of the S−S bond.

The diagonal line (III) is drawn at the maximum energy for reaction 3 and correlates with the appearance of the low E_T and eKE region in Figure 5. Given the structure of the trigonal molecule, this pathway is proposed to correspond to the formation of an O−O bond and the breaking of two S−O bonds. To form the O−O bond, the two oxygen atoms must approach each other by excitation of the OSO bend. The elimination of O_2 by this mechanism is expected to result in considerable vibrational excitation, as previously observed in the ClO_2 molecule.[39] Given KE_MAX = 2.39, energy conservation dictates that production of $S_2 + O_2$ leaves only 0.86 eV of available translational energy. Vibrational excitation of the O_2 product further lowers the available energy, leading to the low E_T plateau in the correlation spectrum. If the cis-OSSO structure is assumed, there is no straightforward explanation for the large shift in E_T that occurs between the two reaction pathways. In both reactions 2 and 3 for the cis-OSSO isomer a cyclic structure must be formed and two bonds must be broken. Figure 6 summarizes the energetics of DPD of $S_2O_2^-$ in terms of the proposed dissociation pathways.

Calculations indicate that the ground state of neutral S_2O_2 is a singlet. If the upper feature in the correlation spectrum is a result of excitation to a repulsive region of this singlet ground state, the observed dissociation to $S(^3P) + SO_2(^1A_1)$ is a spin-forbidden process. Spin-forbidden dissociation pathways have been observed for sulfur-containing compounds such as CS_2,[40] so this type of mechanism is well-known. In the photodissociation of N_3, dissociation to the spin-forbidden $N(^4S) + N_2$ product channel was accompanied by a significant amount of vibrational excitation in N_2.[41] If there is significant vibrational excitation in the SO_2 product upon DPD of $S_2O_2^-$, reducing the energy available for translation, the observed KE_MAX will be lower than the true value. Thus, 2.41 ± 0.06 eV represents an upper bound for the 0 K enthalpy of reaction 2, assuming photodetachment from vibrationally cold anions. If the photodetached anions were vibrationally excited, more energy would be available for translation, possibly increasing the observed KE_MAX. An estimate of the upper limit of the effect of vibrationally excited ("hot") anions can be calculated by assuming an anion temperature of 1000 K, although the actual temperature of the anions is expected to be lower. For this estimate, it is assumed that all anion−neutral transitions have the same Franck−Condon intensity. Relative vibrational populations are calculated on the basis of the DFT/6-311+G(d) frequencies shown in Table 2 (scaled by 0.96[27]). The energy increase is determined from a population-weighted sum of the energy of each vibrational mode. Based on this calculation, an anion temperature of 1000 K could increase the observed KE_MAX by as much as 0.34 eV. However, only those vibrational modes with significant S−S bond stretch character, such as the SS stretch and the SO_2 bend, would be expected to contribute significantly to increased product translational energy. Including only these modes (331 and 490 cm⁻¹) in the calculations results in a potential increase in KE_MAX of 0.13 eV. Taking into account the uncertainty of the vibrational temperature of the anion, a conservative upper bound for the 0 K enthalpy of reaction 2 is 2.41 ± 0.14 eV.

However, the reduction in the apparent KE_MAX resulting from production of vibrationally excited products is likely more significant than the increase arising from photodetachment from hot anions. In the case of the NO⁻−N_2O bond energy, which was determined to be 2.0 ± 0.2 eV using PPC spectroscopy[42] and 0.76 ± 0.10 eV using flowing afterglow tandem mass spectroscopy,[43] the 1.22 eV discrepancy was proposed to arise from the assumption in the PPC experiment that some vibrationally cold products were formed. As with S_2O_2, N_3O_2 exhibits a significant geometry change between the anionic and neutral forms which can result in vibrationally excited products. Since the effect from vibrationally excited products is likely to be larger than the effect from hot anions, it seems reasonable to retain 2.41 eV as the upper limit to the 0 K enthalpy of reaction 2.

Another possible mechanism for the DPD of $S_2O_2^-$, given that photodetachment is not occurring to the stable portion of the S_2O_2 well, is that excitation to a low-lying triplet state of S_2O_2 is responsible for the upper feature in the correlation spectrum, providing a spin-allowed pathway to $S(^3P) + SO_2(^1A_1)$. The lower eKE features, yielding $S(^1D) + SO_2$, and $S_2 + O_2$ products, could then arise from photodetachment to a low-lying excited singlet or a repulsive region of the ground singlet state of S_2O_2 in order to be spin-allowed. As noted by Marsden, the ordering of the singlet and triplet states in the isomers of S_2O_2 is very dependent on the level of theory used,
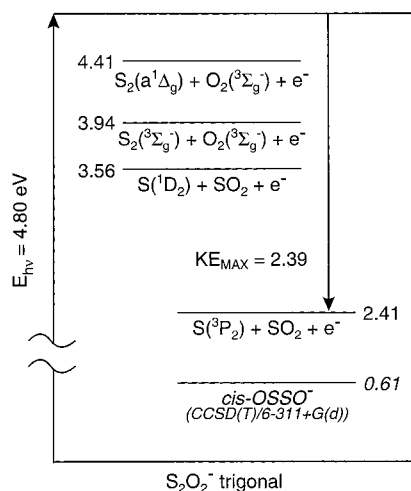
Figure 6. Energetics diagram for DPD of $S_2O_2{}^-$. The calculated energy for cis-OSSO$^-$ over trigonal $S_2O_2{}^-$ at the CCSD(T)/6-311+G(d) level (Table 3) is shown in italics.

so further theoretical work on the energetics of the excited states of S_2O_2 is needed.

6. Conclusions

Photoelectron photofragment coincidence spectroscopy was used to study the energetics and dissociation dynamics of S_2O_2. The experimental results are interpreted in terms of a trigonal isomer of $S_2O_2{}^-$, similar in structure to $SO_3{}^-$. Theoretical calculations predict that the trigonal anion is significantly more stable than the cis-OSSO anion and that the neutral isomers are similar in energy. The vertical detachment energy of the trigonal isomer is determined to be 3.73 ± 0.02 eV. DPD of $S_2O_2{}^-$ at 258 nm occurs to $S(^3P, {}^1D) + SO_2 + e^-$ and $S_2 + O_2 + e^-$. An upper bound of 2.41 ± 0.14 eV is determined for the enthalpy of the reaction $S_2O_2{}^- \rightarrow S + SO_2 + e^-$ at 0 K. The S atom elimination channel is characterized by a large kinetic energy release and a highly parallel photofragment distribution. The dynamics of the O_2 elimination channel are consistent with the formation of vibrationally excited O_2 from a strained intermediate geometry, leading to the low observed E_T. Future experimental studies of $S_2O_2{}^-$ at a higher photon energy could yield more detailed information on the level of vibrational excitation in the O_2 product for the $S_2 + O_2$ dissociation channel. These results, representing the first experimental study of the trigonal form of S_2O_2, may help to elucidate the role of this isomer in the chemical kinetics of SO, giving insight into reactions of this important intermediate.

References and Notes

(1) Levy, A.; Merryman, E. L.; Reid, W. T. *Environ. Sci. Technol.* **1970**, *4*, 653.

(2) Graedel, T. E. *Rev. Geophys. Space Phys. (USA)* **1977**, *15*, 421.

(3) Prinn, R. G. *Geophys. Res. Lett. (USA)* **1979**, *6*, 807.

(4) Lellouch, E.; Strobel, D. F.; Belton, M. J. S.; Summers, M. E.; Paubert, G.; Moreno, R. *Astrophys. J. Lett. (USA)* **1996**, *459*, L107.

(5) Herron, J. T.; Huie, R. E. *Chem. Phys. Lett.* **1980**, *76*, 322.

(6) Harcourt, R. D. *J. Mol. Struct. (THEOCHEM)* **1989**, *186*, 131.

(7) Continetti, R. E. *Int. Rev. Phys. Chem.* **1998**, *17*, 227.

(8) Luong, A. K.; Clements, T. G.; Continetti, R. E. *J. Phys. Chem. A* **1999**, *103*, 10237.

(9) Lovas, F. J.; Tiemann, E.; Johnson, D. *J. Chem. Phys.* **1974**, *60*, 5005.

(10) Marsden, C. J.; Smith, B. J. *Chem. Phys.* **1990**, *141*, 335.

(11) Paulse, C. D.; Poirier, R. A.; Wellington Davis, R. *Chem. Phys. Lett.* **1990**, *172*, 43.

(12) Mathies, P.; Sladky, F. O.; Rode, B. M. *THEOCHEM (Netherlands)* **1982**, *7*, 335.

(13) Mayer, I.; Révész, M. *Inorg. Chim. Acta* **1983**, *77*, L205.

(14) Ng, C. Y. Photoionization, Photoelectron and Photodissociation Studies: Combining Experiment and Theory. In *The Structure, Energetics and Dynamics of Organic Ions*; Baer, T., Ng, C.-Y., Powis, I., Eds.; John Wiley & Sons, Ltd.: Chichester, 1996; p 35.

(15) Cheng, B.-M.; Hung, W.-C. *J. Chem. Phys.* **1999**, *110*, 188.

(16) Hanold, K. A.; Luong, A. K.; Clements, T. G.; Continetti, R. E. *Rev. Sci. Instrum.* **1999**, *70*, 2268.

(17) Robertson, W. H.; Kelley, J. A.; Johnson, M. A. *Rev. Sci. Instrum.* **2000**, *71*, 4431.

(18) Campargue, R. *J. Chem. Phys.* **1970**, *52*, 1795.

(19) Clements, T. G.; Luong, A. K.; Deyerl, H.-J.; Continetti, R. E. *J. Chem. Phys.* **2001**, *114*, 8436.

(20) Hanold, K. A.; Luong, A. K.; Continetti, R. E. *J. Chem. Phys.* **1998**, *109*, 9215.

(21) Frisch, M. J.; Trucks, G. W.; Schlegel, H. B.; Scuseria, G. E.; Robb, M. A.; Cheeseman, J. R.; Zakrzewski, V. G.; Montgomery, J. A., Jr.; Stratmann, R. E.; Burant, J. C.; Dapprich, S.; Millam, J. M.; Daniels, A. D.; Kudin, K. N.; Strain, M. C.; Farkas, O.; Tomasi, J.; Barone, V.; Cossi, M.; Cammi, R.; Mennucci, B.; Pomelli, C.; Adamo, C.; Clifford, S.; Ochterski, J.; Petersson, G. A.; Ayala, P. Y.; Cui, Q.; Morokuma, K.; Malick, D. K.; Rabuck, A. D.; Raghavachari, K.; Foresman, J. B.; Cioslowski, J.; Ortiz, J. V.; Stefanov, B. B.; Liu, G.; Liashenko, A.; Piskorz, P.; Komaromi, I.; Gomperts, R.; Martin, R. L.; Fox, D. J.; Keith, T.; Al-Laham, M. A.; Peng, C. Y.; Nanayakkara, A.; Gonzalez, C.; Challacombe, M.; Gill, P. M. W.; Johnson, B. G.; Chen, W.; Wong, M. W.; Andres, J. L.; Head-Gordon, M.; Replogle, E. S.; Pople, J. A. *Gaussian 98*, Revision A.7; Gaussian, Inc.: Pittsburgh, PA, 1998.

(22) Lee, C. T.; Yang, W. T.; Parr, R. G. *Phys. Rev. B* **1993**, *37*, 785.

(23) Becke, A. D. *J. Chem. Phys.* **1993**, *98*, 5648.

(24) Krishnan, R.; Binkley, J. S.; Seeger, R.; Pople, J. A. *J. Chem. Phys.* **1980**, *72*, 650.

(25) Pople, J. A.; Head-Gordon, M.; Raghavachari, K. *J. Chem. Phys.* **1987**, *87*, 5968.

(26) Scuseria, G. E.; Janssen, C. L.; Schaefer, H. F., III. *J. Chem. Phys.* **1988**, *89*, 7382.

(27) Scott, A. P.; Radom, L. *J. Phys. Chem.* **1996**, *100*, 16502.

(28) Dobrin, S.; Boo, B. H.; Alconcel, L. S.; Continetti, R. E. *J. Phys. Chem. A* **2000**, *104*, 10695.

(29) Deyerl, H.-J.; Alconcel, L. S.; Continetti, R. E. *J. Phys. Chem. A* **2001**, *105*, 552.

(30) Nimlos, M. R.; Ellison, G. B. *J. Phys. Chem.* **1986**, *90*, 2574.

(31) Wang, X. B.; Nicholas, J. B.; Wang, L. S. *J. Phys. Chem. A* **2000**, *104*, 504.

(32) Li, R.-J.; Hanold, K. A.; Garner, M. C.; Luong, A. K.; Continetti, R. E. *Faraday Discuss.* **1997**, 115.

(33) Sherwood, C. R.; Continetti, R. E. *Chem. Phys. Lett.* **1996**, *258*, 171.

(34) Busch, G. E.; Wilson, K. R. *J. Chem. Phys.* **1972**, *56*, 3655.

(35) Zare, R. N. *Mol. Photochem.* **1972**, *4*, 1.

(36) Chase, M. W., Jr.; Davies, C. A.; Downy, J. R., Jr.; Frurip, D. J.; McDonald, R. A.; Syverud, A. N. *JANAF Thermochemical Tables*, Supplement 1 ed.; American Institute of Physics: New York, 1985; Vol. 14.

(37) Li, R.-J.; Continetti, R. E. *J. Phys. Chem. A*, submitted.

(38) Li-Shiun, C.; Cheng, I. L.; Yuan-Pern, L. *J. Chem. Phys.* **1996**, *105*, 9454.

(39) Davis, H. F.; Lee, Y. T. *J. Chem. Phys.* **1996**, *105*, 8142.

(40) Mank, A.; Starrs, C.; Jego, M. N.; Hepburn, J. W. *J. Chem. Phys.* **1996**, *104*, 3609.

(41) Continetti, R. E.; Cyr, D. R.; Osborn, D. L.; Leahy, D. J.; Neumark, D. M. *J. Chem. Phys.* **1993**, *99*, 2616.

(42) Resat, M. S.; Zengin, V.; Garner, M. C.; Continetti, R. E. *J. Phys. Chem. A* **1998**, *102*, 1719.

(43) Torchia, J. W.; Sullivan, K. O.; Sunderlin, L. S. *J. Phys. Chem. A* **1999**, *103*, 11109.